doi:10.3788/gzxb20174612.1211003

侧面遮拦式日晕光度计的杂散光理论分析

孙明哲[1],张红鑫[2],刘维新[1],夏利东[1]

(1 山东大学 空间科学研究院 山东省光学天文与日地空间环境重点实验室,山东 威海 264209)

(2 中国科学院长春光学精密机械与物理研究所,长春 130033)

摘 要:提出了一种侧面遮拦结构的日晕光度计,在镜筒内通过设置多层挡板结构逐层抑制处于内视场的挡板边缘衍射光,同时采用倾斜布置的上挡板结构抑制处于外视场的入射窗口边缘衍射光和侧壁散射光.建立数学模型对这些杂散光抑制挡板进行了仿真计算,结果表明,优化各挡板的几何参数后,日晕光度计的设计视场可达3.5~10个太阳半径,视场内的杂散光水平均可低于10^{-8}平均太阳亮度.相对于高山天文台的日晕光度计在4~8个太阳半径的视场内总杂散光达到10^{-7}平均太阳亮度,该日晕光度计扩展了可观测视场,并使杂散光抑制提高了一个量级.

关键词:物理光学;杂散光;散射;衍射;日晕光度计;大气散射

中图分类号:O436 **文献标识码**:A **文章编号**:1004-4213(2017)12-1211003-9

Theoretical Stray Light Analysis of Side-baffled Sky Brightness Photometer

SUN Ming-zhe[1], ZHANG Hong-xin[2], LIU Wei-xin[1], XIA Li-dong[1]

(1 *Shandong Provincial Key Laboratory of Optical Astronomy and Solar-Terrestrial Environment, Institute of Space Sciences, Shandong University, Weihai* 264209, *China*)

(2 *Changchun Institute of Optics, Fine Mechanics and Physics, Chinese Academy of Sciences, Changchun* 130033, *China*)

Abstract: A sky brightness photometer with a side-baffled structure, which adopts multibaffles to suppress diffracted stray light layer-by-layer in the inner field of view, is proposed. In addition, specially designed upper baffles block both scattered and diffracted stray light in the outer field of view. A mathematical model is established to simulate the baffles, and calculated results show that the field of view of the photometer can be designed to be 3.5~10 solar radii by optimizing the geometric parameters of the baffles. The stray light in the full field of view can be suppressed effectively to less than 10^{-8} of the mean solar brightness. Compared with the High Altitude Observatory, which has a sky brightness monitor with a field of view of 4~8 solar radii and a stray light level of 10^{-7} of the mean solar brightness, the proposed photometer expands the observable field of view and improves the stray light suppression level by over an order of magnitude.

Key words: Physical optics; Stray light; Scattering; Diffraction; Sky brightness photometer; Atmospheric scattering

OCIS Codes: 290.2648; 050.1940; 120.4640

Foundation item: The National Natural Science Foundation of China (No.41627806), the Shandong Provincial Natural Science Foundation, China (No. BS2014SF018)

First author: SUN Ming-zhe (1984-), male, lecturer, Ph.D. degree, mainly focuses on stray light design and analysis. Email: sunmingzhe@sdu.edu.cn

Corresponding author: LIU Wei-xin (1980-), male, associate research fellow, Ph.D. degree, mainly focuses on laser and space optical instrument design and manufacture. Email: liuwx@sdu.edu.cn

Received: May.27, 2017; **Accepted**: Sep.11, 2017

0 Introduction

Sky brightness photometers can detect sky-scattered light caused by sunlight interacting with particles distributed in the Earth's atmosphere. Such photometers are used to determine whether one location can meet the requirements of a faint solar corona observation by measuring the sky brightness near the sun. Moreover, long-term sky brightness observational data, particularly for precipitable water vapor and aerosol content, can be used while studying the global climate[1-2]. In addition, photometers can provide great reference values in site investigations of solar telescopes and astronomical instruments for night-time observation[3]. Currently, there are two major types of sky brightness photometers applied globally: the Evans Sky Photometer (ESP)[4-5], which has been used at many solar observatories, and the Sky Brightness Monitor (SBM)[6], which was originally developed for the Advanced Technology Solar Telescope (ATST) site survey. An SBM-like photometer was also fabricated at the Yunnan Observatory of the Chinese Academy of Sciences[7], whose performance was enhanced by using an advanced CCD. Presently, SBM photometers are placed in several solar observatories for age-long sky brightness measurements. The photometer developed at the Yunnan Observatory has been used for sky brightness measurements at various locations such as Dali and Jiaozi mountain[8-9].

The sky field of view (FOV) of the ESP is 1.6～4.4 $R_\odot$ ($R_\odot$ being the solar radius), with a structure similar to that of an externally occulted coronagraph. The ESP can suppress the stray light to a fraction of a millionth of the mean solar brightness, but it needs a specially polished high-quality objective lens[4]. However, this type of sky brightness photometer can only be used at a single wavelength and is not suitable for measuring the content of aerosol and integrated water vapor in the Earth's atmosphere. In addition, this photometer is not suitable for age-long automatic observation owing to the need for manual manipulation. Most importantly, the fabrication cost of the ESP is relatively high and the structure is complicated[6]. The SBM has a simplified, externally occulted structure with a sky field of view of 4～8 $R_\odot$. It adopts an external occulter, wound with multilayer O-rings, to eliminate the diffraction light in the inner field. Towards its exterior, the stray light scattered by the lens barrel wall is eliminated by baffle rings. The stray light level of the SBM is about 10^{-7} $B_\odot$ ($B_\odot$ being the average brightness of the solar disk), whereas the stray light at the edge of the inner and outer fields of view is comparatively high, about 10^{-4} $B_\odot$. After passing through the aperture centered at the external occulter and two ND2 attenuation filters, the direct sunlight drops to a magnitude of 10^{-4} $B_\odot$, and then shines into the optical system. The SBM has advantages such as high stability, automatic observation, and low cost. However, the diffraction light in both the inner and outer fields is strong, restraining the measurement of sky brightness more precisely at the edge of the inner and outer fields. Bright rings can be seen in both fields of the images taken by the SBM and, therefore, the actual inner field is only 4 $R_\odot$.

This paper is focused on improving the level of stray light suppression of the photometer under low-cost conditions. The most important stray light in the SBM is the diffracted light in both the inner and outer fields of view. In terms of suppressing diffracted stray light, the side-baffled structure adopted by the Heliosphere Imager (HI) on board the STEREO (Solar Terrestrial Relations Observatory) mission can exhibit better performance than a center-occulted structure[10-11]. To suppress the diffracted stray light, two methods are adopted in our photometer. One method uses a set of front baffles of a side-baffled structure to suppress stray light in the inner field. The other method adopts a set of upper baffles blocking layer-by-layer the stray light in the outer field. Using these methods, a side-baffled sky brightness photometer (SSBP) was designed to achieve a field of view of 3.5～10 $R_\odot$ with a stray light level of 10^{-8} $B_\odot$. Compared to the SBM, whose stray light level is 10^{-7} $B_\odot$ in the sky field of view of 4～8 $R_\odot$, the present photometer expands the observable field of view and improves the level of stray light suppression by over an order of magnitude. Because the sky brightness has rotational symmetry around the sun, the loss of circumferential field of view caused by the side-baffled structure is acceptable.

1 Overall structure design of the SSBP

The side-baffled front baffles in the STEREO-HI suppress stray light to below 10^{-9} $B_\odot$ (the inner

FOV is 15 $R_\odot$), which has led to the big success of the HI[11]. When designing the present photometer, we focused on the advantages of the SBM and the side baffles in the STEREO-HI, and on achieving a further reduction of stray light in both the inner and outer fields of view. The overall design of the SSBP is shown in Fig. 1. Sunlight and sky-scattered light comes into the lens barrel from the left side. Sky-scattered light enters the lens barrel at an oblique angle over the top of the front baffles and is then imaged on the image plane by the objective lens. The diffraction light in the outer field and scattered light on the lens barrel wall are suppressed by the upper baffles while the lower baffles mainly suppress the scattered light on the lower barrel wall. This design is similar to that of common baffles to eliminate stray light[12-14].

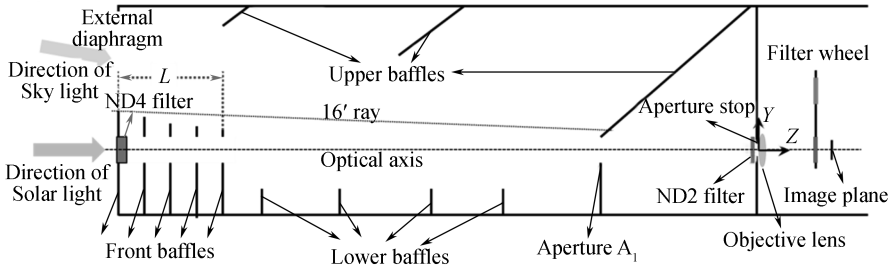

Fig.1 Schematic of the SSBP

An achromatic doublet with a focal length of 50 mm, purchased from the EdmundCorporation was adopted as the objective lens. The clear aperture was reduced to 4 mm to achieve easier suppression of stray light. However, this leads to a larger diameter of the Airy disk and a lower spatial resolution. As the main purpose of the SSBP is to measure the sky brightness parameters, the low resolution (about 56", 2×2 binned) and the larger airy disk have little impact on the SSBP performance.

2 Computation of diffraction and optimal design of front baffles

2.1 Computation of diffractionfrom front baffles

Diffractionfrom front baffles is calculated using Fresnel integrals[15] and the Fresnel-Kirchhoff diffraction formula[15-16], where the complex amplitude of diffracted light $U(x, y)$ in the x and y coordinates in the observing plane is respectively given by

$$\begin{cases} U(x,y)=\dfrac{U_0\exp(\mathrm{j}kz)}{2\mathrm{j}}(1+\mathrm{j})\left\{\left[\dfrac{1}{2}-C(\beta_1)\right]+\mathrm{j}\left[\dfrac{1}{2}-S(\beta_1)\right]\right\} \\ C(x)=\displaystyle\int_0^x\cos\left(\frac{\pi\xi^2}{2}\right)\mathrm{d}\xi \\ S(x)=\displaystyle\int_0^x\sin\left(\frac{\pi\xi^2}{2}\right)\mathrm{d}\xi \end{cases} \tag{1}$$

$$U(x,y)=\frac{\exp(\mathrm{j}kz)}{\mathrm{j}\lambda z}\iint_s U_1(\xi,\eta)\exp\left\{\mathrm{j}\frac{k}{2z}[(x-\xi)^2+(y-\eta)^2]\right\}\mathrm{d}\xi\mathrm{d}\eta \tag{2}$$

where $\beta_1\equiv\left(\dfrac{2}{\lambda z}\right)^{\frac{1}{2}}(\eta_1-y)$, η_1 is the y coordinate of the edge of the semi-infinite screen, λ is the wavelength, $k=2\pi/\lambda$, z is the distance from the observation point to the diffraction screen, and ξ and η are the coordinates in the diffraction screen plane. Eq.1 uses Fresnel integrals to compute the diffraction of a semi-infinite screen.

Diffraction fromthe first front baffle R_1 shown in Fig. 2 is calculated by using Fresnel integrals directly. Diffraction from the second front baffle R_2 is divided into contributions from two regions, as shown in Fig. 2. The first region (dashed-line region in Fig. 2) is next to R_2 and diffraction from R_2 is influenced by diffraction from R_1. The second region (dotted line region in Fig. 2) is a distance away from R_2 and the influence of diffraction from R_1 can be neglected. Therefore, the former can be calculated by using Fresnel integrals while the latter can be calculated by using Fresnel-Kirchhoff diffraction formula. Using this method, an infinite integral is converted into a sum of finite integrals and plus the Fresnel diffraction contribution from a semi-infinite opaque screen.

To prove the reliability of this algorithm, we applied it to compute the diffraction brightness B from

the HI front baffles and compared our results with the HI experimental and theoretical data[10-11], as shown in Fig. 3. Our calculated results (red line) are in better accord with the HI measurements than the HI theoretical results for field of view between 0 and −1.5°.

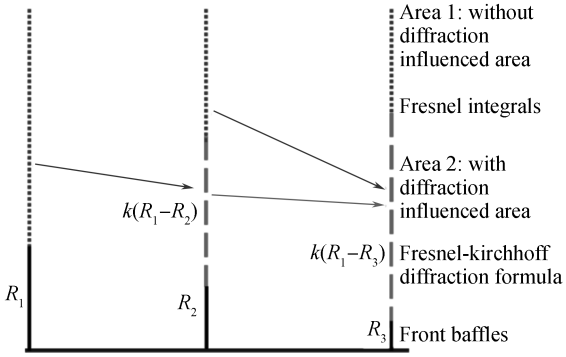

Fig.2 Algorithm of diffraction from front baffles

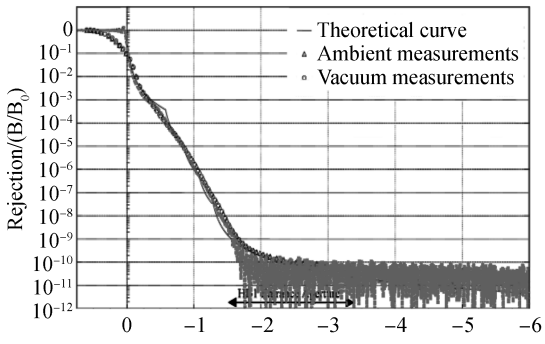

Fig.3 Comparison of the brightness calculated by using our algorithm with the HI experimental and theoretical data

2.2 Optimal design of front baffles

In order to achieve much lower stray light than that inthe SBM, the front baffles of the SSBP were designed by adopting multivane baffles instead of an external occulter, as shown in Fig. 1. Two schemes were considered to determine the heights and separations of the parallel multivane: an equal-height-difference scheme and an equal-angle-difference scheme. In the former scheme, the height differences between any two adjacent baffles are the same and this has been the scheme used in most traditional externally occulted coronagraphs. In the latter scheme, discussed by Buffington[17], the angular differences between any two adjacent baffles are the same. Fig. 4 shows an example of the latter using three parallel front baffles, where α represents a fully baffled inner field angle β is the 16-arcminute divergence half angle of the Sun, and $\Delta\alpha=(\alpha-\beta)/3$. The diffraction intensity with a five-knife-edge-vane system was calculated using the two schemes, as shown in Fig. 5. Results indicate that the intensity obtained using the equal-angle-difference scheme is around half of that obtained using the equal-height-difference scheme. Therefore, the equal-angle-difference schemewas adopted.

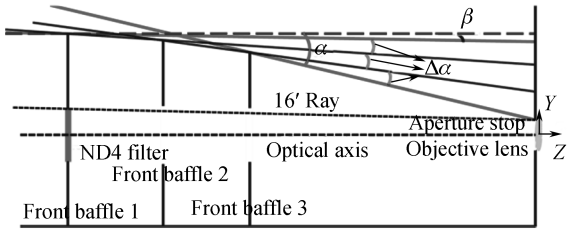

Fig.4 Equal-angle-difference design of front baffles

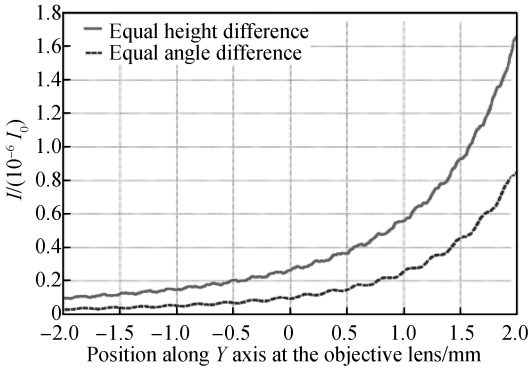

Fig. 5 Comparison between the diffraction intensities obtained using the equal-height-difference and the equal-angle-difference schemes

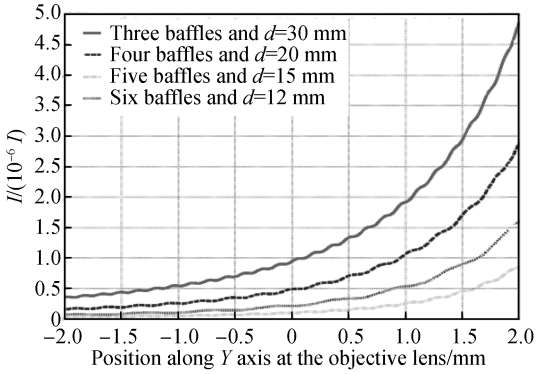

Fig.6 Comparison of diffraction intensity for 3～6 baffles

The calculated diffraction intensity for various numbers of baffles is shown in Fig. 6 under the

assumption that the distance between the first and last baffle (denoted by L in Fig. 1) is the same and equal to 60 mm. The figure shows that the diffraction intensity decreases as the number of baffles increases from 3 to 5. However, the diffraction intensity derived from six baffles is larger than that from five baffles. Thus, we chose five vanes to design the photometer front baffles.

In addition to the height of the front baffle vanes, the distance between adjacent baffles is crucial in reducing stray light. Since the distance between any two adjacent baffles d is the same, the diffraction intensity within the aperture of the objective lens is expected to decrease for increasing values of d[17]. Note that the abovementioned calculation is under the condition that the distance between the last vane and the objective is constant, in which case the overall length of the instrument increases as d increases.

Fig. 7 displays the calculated intensity distribution of diffracted light around the objective lens for different distances d between any two adjacent baffles, assuming that the distance between the first front baffle andthe objective lens that determines the overall length of the instrument is fixed. The figure shows that the diffraction intensity decreases as d increases. However, the rate of change of the diffraction intensity is less pronounced for values of d larger than 25 mm. Since the overall length of the instrument is fixed, as the value of d increases the last front baffles become closer to the objective lens , and thus these baffles become more out of focus on the image plane. A larger out-of-focus area leads to more diffused imaging of the diffraction light, which impacts the observation of the inner field. Therefore, based on the above calculations, the interval distance of the front baffles was chosen to be 25 mm.

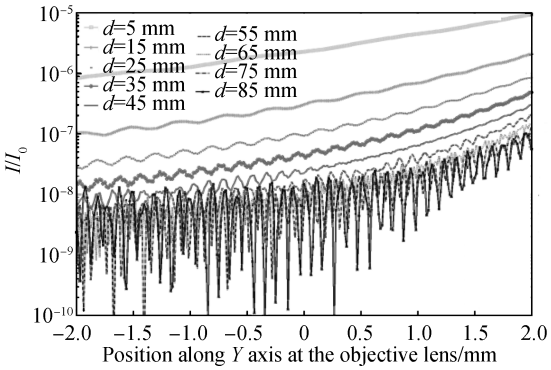

Fig. 7 Diffraction intensity at the objective lens with different distances d between any two adjacent front baffles

The calculated upper edge positions of the front baffles are listed in Table 1. The coordinate system, with the center of the front surface of the lens as the origin, is shown in Fig. 1. Based on scalar diffraction theory, the average diffraction intensity of the front baffles within the aperture of the objective lens was determined to be 1.3×10^{-6} $B_\odot$. This diffraction light was focused by the objective lens at around 2.53 $R_\odot$ on the image plane. In order to determine the relative value between the sky brightness and corona brightness, the SBM adopted two ND2 (nominal optical density of 2) attenuators at the center of its external occulter so that direct sunlight would be attenuated by 10^{-4} before entering the optical system[6]. The same method was adopted in our photometer. The diameter of the attenuator apertures should allow the rays from each point of the sun to illuminate the aperture of the objective lens without any blocking by the aperture edge. Therefore, we estimated that the clear aperture of the attenuator should be larger than 12 mm, and was chosen to be 13 mm, for which the sunlight brightness is expected to be relatively uniform on the image plane.

Table 1 Coordinates of upper edges of front baffles (Coordinate system is shown in Fig.1)

	Z/mm	Y/mm
Front Baffle 1	−860	9.77
Front Baffle 2	−835	9.63
Front Baffle 3	−810	9.47
Front Baffle 4	−785	9.28
Front Baffle 5	−760	9.07

3 Structure design of external diaphragm and upper baffles

The main function of the external diaphragm and upper baffles is torestrain the scattered stray light in the outer field and lens barrel wall. In addition, the upper baffles can suppress the diffracted stray light from the external diaphragm edge. In general, diffracted light from the external diaphragm is suppressed

by blocking at the image plane. However, we developed a new approach to suppress the diffracted light from the external diaphragm using the upper baffles shown in Fig. 8. Point D in the figure is the lower edge of upper baffle 3 and is required to be within the umbra of the front baffles without blocking the rays in the outer field. In this case, there is no direct sunlight illuminating point D so the diffraction light on the edge can be neglected. Therefore, point D should be located within the shadow area indicated in the figure. Using the coordinate system in Fig. 1, the cross-point H was calculated to be at (0, 6.19 mm, −89.87 mm) and the coordinates of point D were chosen to be (0, 5.8 mm, −81.6 mm).

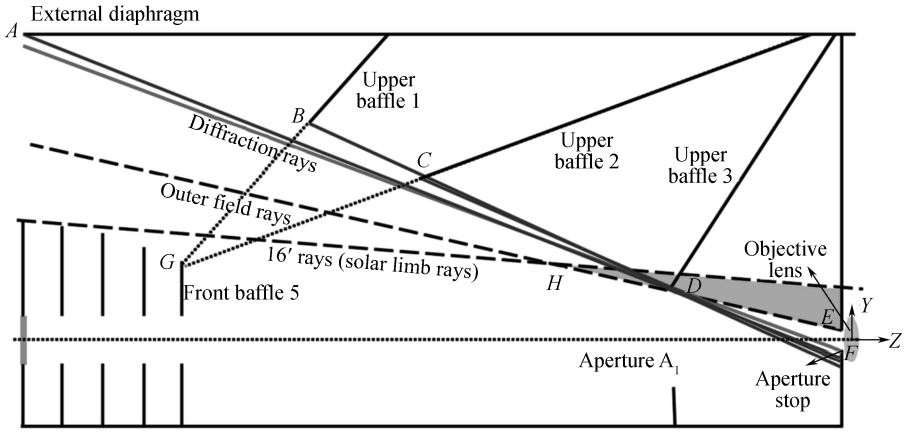

Fig.8 Schematic of the size design for upper baffles

Upper baffle 3 can block the diffracted stray light from the external diaphragm and upper baffles 1 and 2. The main function of upper baffle 2 is to reduce the scattered light of direct sunlight on upper baffle 3 and the wall of the lens barrel. The function of upper baffle 1 is similar to that of upper baffle 2 and the light suppression mechanism is shown by the extended dotted lines in Fig. 8, which intersect with point G. Thus, the scattered light on the surfaces of upper baffles 1 and 2 will be unable to irradiate on the back surface of front baffle 5. Hence, after scattering at least three times, light can reach the objective lens.

In order to suppress the diffraction light from upper baffles 1 and 2, their lower edge should be positioned above the connecting line between point F and D in Fig. 8 (red line). In this case, diffraction from the edge of upper baffles 1 and 2 is blocked by upper baffle 3. Likewise, point A is above the connecting line between points F and D. Using the above design, the edge positions were calculated and the resulting values are listed in Table 2. The total intensity distribution for diffraction from the external diaphragm and upper baffles 1, 2, and 3 is shown in Fig. 9 as a function of the field of view R. The figure shows that the brightness of the diffraction light within the FOV range of 3～10 $R_\odot$ is below 10^{-8} $B_\odot$. As the other two sides of the external diaphragm are above the aperture of the objective lens, the vertical directions of their edges avoid the objective lens aperture. Thus, the edge diffraction intensity can be neglected[18-19].

Table 2 Coordinates of upper edges of front baffles (Coordinate system is shown in Fig.1)

	Z/mm	Y/mm
External Diaphragm (A)	−860	81
Upper Baffle 1 (B)	−700	72
Upper Baffle 2 (C)	−433	40
Upper Baffle 3 (D)	−81.6	5.8

When deglossing paint is applied to all surfaces, the totalamount of scattered light is below 1% on each surface i.e., more than 99% is absorbed. According theory analysis, the brightness of light scattered from upper baffles 1 and 2 can be reduced to below 10^{-8} $B_\odot$ after scattering three times. According to the scattering theory, the scattered intensity decreases with increasing scattering angle [20-21]. The dip angle of upper baffle 3 is maximized to minimize the scattered light brightness. Moreover, the majority of the front surface of upper baffle 3 is blocked by upper baffle 2 to lower the scattered light brightness. The brightness of the scattered light was estimated to be lower than 1 0^{-6} $B_\odot$. Although the brightness of

the scattered light is not very low, only a little of the energy of this scattered light is imaged in the FOV range of 3.5 ~ 10 $R_\odot$. Using the above design, the brightness of the scattered light caused by direct sunlight can be reduced by the external diaphragm and upper baffles to below 10^{-8} $B_\odot$ for the FOV range of 3.5~10 $R_\odot$.

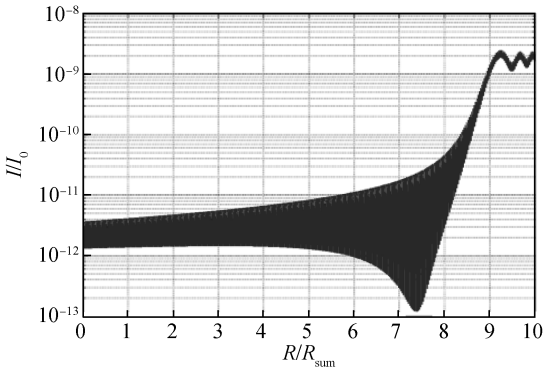

Fig.9 Total diffraction intensity distribution from the external diaphragm and upper baffles on the image plane

4 Results and analysis of overall design

The SSBP was designed considering all of the calculations above and the overall structure (a cuboid with overall dimensions of 1 2 0 mm × 150 mm×1 000 mm) is shown in Fig.10. The intensity distribution derived from the simulations for light diffraction from the front baffles and upper baffles on the image plane is shown in Fig. 11. Within the SSBP field of view (3.5~10 $R_\odot$), the stray light brightness is lower than 10^{-8} $B_\odot$, which is much better than that of the SBM and can improve the measuring precision and meet the sky brightness measuring requirements.

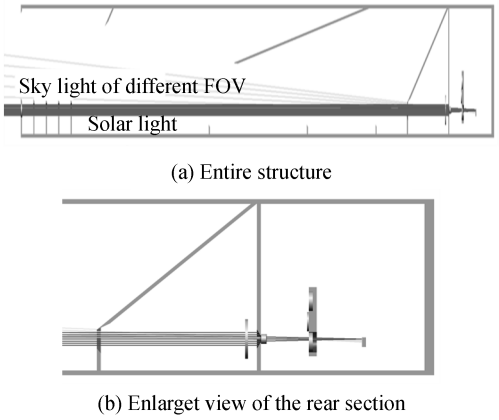

Fig.10 Overall structure diagram of the SSBP

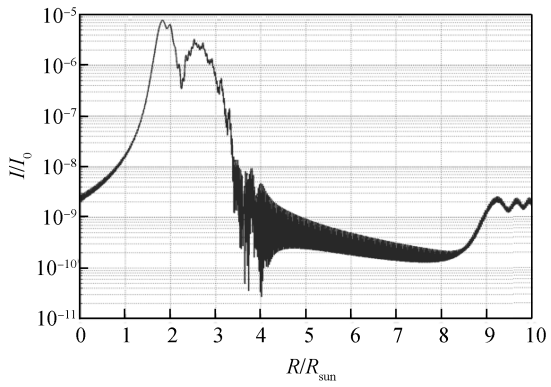

Fig.11 Total diffraction intensity distribution on the image plane

Vignetting, defocus of the last front baffle, and diffraction are the main factors that influence the inner field of the SSBP. Based on the method used by Lin and Penn[6], the fully baffled inner field angle α of the SSBP is 2 $R_\odot$, and the inner field angle β without vignetting is 3.12 $R_\odot$. However, 50% vignetting is acceptable for sky brightness detection. In our case, the inner field angle is 2.56 $R_\odot$ for 50% vignetting. Thus, the field of view range actually influenced by vignetting is between 2 and 2.56 $R_\odot$.

Theeffects of defocus and diffraction are entangled. Diffraction determines the total diffracted light energy incident upon the objective lens whereas defocus determines the extent of diffusion of the diffracted light at the image plane. The Zemax parameters provided by the Edmund Corporation were adopted to calculate the defocus. The edge of front baffle 5 was imaged at around 0.588 mm below the optical axis, which is equivalent to a field of view of 2.53 $R_\odot$. The root mean square (RMS) radius of the blur spot was 121 μm, corresponding to a field of view of 0.52 $R_\odot$. This means that about 68% of the diffraction energy from the front baffle is condensed in the field of view range of 2.01~3.05 $R_\odot$.

Fig.11 shows the diffraction intensity distribution at the image plane. The calculated ranges of the sky field of view are 1.5~2.93 $R_\odot$ for diffraction intensities above 10^{-6} $B_\odot$, and 0.8~3.5 $R_\odot$ for diffraction intensities above 10^{-8} $B_\odot$. The inner field of view could be further lowered by increasing the length of the SSBP along the *z*-axis and decreasing the aberration. Under the same diffraction angle and wavelength, an increased length could lead to a further decrease in diffraction intensity[22] and can further decrease the defocus of the front baffle. Moreover, vignetting could also be reduced by increasing the length of the SSBP. Fig. 11 shows that, for a field of view range of 3~3.5 $R_\odot$, the diffraction intensity decreases rapidly from 10^{-6} $B_\odot$ to below 10^{-8} $B_\odot$. The intensity increase for a field of view range of 8~10 $R_\odot$ is a result of

diffraction from the upper baffles. Therefore, the intensity is below 10^{-8} $B_{\odot}$ in the field of view range of 3.5～10 $R_{\odot}$.

Fig. 12 compares the fields of view of the SBM and SSBP, where the background corresponds to the SBM[23] and the three highlighted gray arc regions are the FOVs used to measure the sky brightness. The red and yellow areas are the SSBP image regions. The red areas is used to image the attenuated sun whereas the yellow area is the FOV used for the SSBP to make measurements. The brightness of stray light in the entire area is lower than 10^{-8} $B_{\odot}$ and the photometer is sufficiently precise to measure the sky brightness in spite of machine and assembling errors.

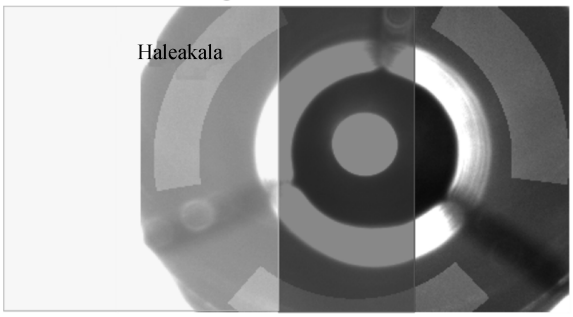

Fig.12 Comparison between the FOVs for the SBM and the SSBP

Finally, people who work on site surveys prefer smaller equipment. To satisfy this need, we have calculated that with the same field of view of the SBM, the dimensions of the SSBP is expected to be smaller than 750 mm×70 mm×70 mm. Furthermore, for a field of view in the range of 5～10 $R_{\odot}$, the dimensions of the SSBP is expected to be 600 mm×70 mm×70 mm. The stray light is expected to be lower than 10^{-8} $B_{\odot}$ for all the SSBP fields of view.

5 Conclusion

In this paper, a new type of side-baffled sky brightness photometer (SSBP) was designed to achieve high stray-light suppression. By adopting front baffles similar to those of the STEREO-HI, the brightness of diffracted stray light inside the inner field can be suppressed to a level lower than 10^{-8} $B_{\odot}$ for fields of view above 3.5 $R_{\odot}$. In addition, upper baffles were specially designed to eliminate the influence of scattered light into the lens barrel derived from direct sunlight and diffraction from the edges of the upper baffles. Using the design proposed in this article, the SSBP can achieve a stray light brightness level of 10^{-8} $B_{\odot}$ in a sky field of view range of 3.5～10 $R_{\odot}$.

References

[1] TRIPATHI S N, DEY S, CHANDEL A, *et al*. Comparison of MODIS and AERONET derived aerosol optical depth over the Ganga Basin, India[J]. *Annales Geophysicae*, 2005, **23**(4): 1093-1101.

[2] RANJAN R R, GANGULY N D, JOSHI H P, *et al*. Study of aerosol optical depth and precipitable water vapour content at Rajkot, a tropical semi-arid station[J]. *Indian Journal of Radio & Space Physics*, 2007, **36**(1): 27-32.

[3] DAI Cong-ming, ZHANG Zhi-yong, MA Li, *et al*. Measuring and analysis of atmospheric transfer and environment background character on infrared telescope site[J]. *Infrared and Laser Engineering*, 2016, **45**(12): 1204005.

[4] EVANS J W. A photometer for measurement of sky brightness near the sun[J]. *Journal of the Optical Society of America*, 1948, **38**(38): 1083-1085.

[5] LIU Yu, GAO Jing-hua, PEI Xiao-xing. Principle of measurement with an Evans visual sky photometer[J]. *Astronomical Research and Technology*, 2012, **9**(3): 290-294.

[6] LIN H, PENN M J. The advanced technology solar telescope site survey sky brightness monitor[J]. *Publications of the Astronomical Society of the Pacific*, 2004, **116**(821): 652-666.

[7] LIU Nian-ping, LIU Yu, SHEN Yuan-deng, *et al*. Measurement of sky brightness and suppression of scattering in sky brightness monitor[J]. *Acta Astronomica Sinica*, 2011, **52**(2): 160-170.

[8] LIU Y, SHEN Y D, ZHANG X F, *et al*. Using a new sky brightness monitor to observe the annular solar eclipse on 15 January 2010[J]. *Solar Physics*, 2012, **279**(2): 561-572.

[9] SONG Teng-fei, LIU Sun-qing, ZHANG Xue-fei. Measurement of total precipitable water in atmosphere with sky brightness monitor[J]. *Meteorological Science and Technology*, 2013, **41**(1): 46-50.

[10] HOWARD R A, MOSES J D, SOCKER D G, *et al*. Sun earth connection coronal and heliospheric investigation (SECCHI)[J]. *Space Science Reviews*, 2008, **29**(1): 2017-2026.

[11] EYLES C J, HARRISON R A, DAVIS C J, *et al*. The heliospheric imagers on board the STEREO mission[J]. *Solar Physics*, 2009, **254**(2): 387-445.

[12] SMITHW J, Modern optical engineering: the design of optical systems, fourth edition[M]. New York, McGraw-Hill, 2000,147-151.

[13] LIAO Zhi-Bo, JIAO Wen-chun, FU Rui-min. Veiling glare index calculation for refract optical system[J]. *Acta*

Photonica Sinica, 2011, **40**(3): 424-427.

[14] CHEN Xue, SUN Chuang, XIA Xin-lin. Bidirectional reflection characteristics of honeycomb cell in baffle[J]. *Acta Photonica Sinica*, 2012, **41**(3): 353-357.

[15] HECHT E. Optics 4th Edition[M]. New York, Addison Wesley, 2002, P498 for the Fresnel Integrals and P511 for the Fresnel-Kirchhoff diffraction formula.

[16] JI Jia-rong. A course in advanced optics: basic electromagnetic theory in optics[M]. Beijing, Science Press, 2007, P189 (in Chinese).

[17] BUFFINGTON A, JACKSON B V, KORENDYKE C M. Wide-angle stray-light reduction for a spaceborne optical hemispherical imager[J]. *Applied Optics*, 1996, **35**(34): 6669-6673.

[18] SUN M, ZHANG H, BU H, *et al*. Computation of the diffracted field of a toothed occulter by the semi-infinite rectangle method.[J]. *Journal of the Optical Society of America A Optics Image Science & Vision*, 2013, **30**(10): 2140-2149.

[19] SUN Ming-zhe, ZHANG Hong-xin, LU Zhen-wu, *et al*. Design and diffraction intensity test of the toothed occulter[J]. *Optics and Precision Engineering*, 2015, **23**(1): 70-77.

[20] STOVERJ C. Optical scattering: measurement and analysis, third edition[M]. New York, McGraw-Hill, 1990.

[21] NELSON P G. An analysis of scattered light in reflecting and refracting primary objectives for coronagraphs[M]. Coronal Solar Magnetism Observatory Technical Note, 2006.

[22] LANDINI F, ROMOLI M, BACCANI C, *et al*. Scaled-model guidelines for formation-flying solar coronagraph missions[J]. *Optics Letters*, 2016, **41**(4): 757-760.

[23] PENN M J, LIN H S, SCHMIDT A M, *et al*. Extinction and sky brightness at two solar observatories[J]. *Solar Physics*, 2004, **220**(1): 107-120.